Journal of the Taiwan Institute of Chemical Engineers 147 (2023) 104937

Contents lists available at ScienceDirect

Journal of the Taiwan Institute of Chemical Engineers

journal homepage: www.journals.elsevier.com/journal-of-the-taiwan-institute-of-chemical-engineers

Improved carbon steel corrosion characteristics in static and hydrodynamic HCl media by two novel N_2O_2 ligands: Experimental and theoretical studies

Saeid Karimi [a,*], Majid Rezaeivala [b,*], Mohammadreza Mokhtare [a], Gamze Tuzun [c], Koray Sayin [c]

[a] Department of Metallurgy and Materials Engineering, Hamedan University of Technology, Hamedan 6516913733, Iran
[b] Department of Chemical Engineering, Hamedan University of Technology, Hamedan 6516913733, Iran
[c] Faculty of Science, Department of Chemistry, Sivas Cumhuriyet University, Sivas 58140, Turkey

ARTICLE INFO

Keywords:
Schiff base
Synthesis
Carbon-steel
Acid corrosion
Corrosion inhibition
Electrochemical analysis
Modeling studies

ABSTRACT

Background: Expanding the use of carbon steel in various industrial operations is always associated with challenges due to many engineering factors in the selection of materials. However, carbon-steel corrosion is a significant challenge in many industries, particularly the oil and gas sector.

Methods: This study created and employed two novel N_2O_2 ligands to prevent simple carbon steel from corroding in static and dynamic hydrochloric acid solutions. Corrosion tests were performed in none, 50, 100, and 250 ppm of the new compounds. Therefore, immersion, potentiodynamic polarization (PDP), and electrochemical impedance spectroscopy (EIS) tests were used to investigate the anti-corrosion effect. In addition, the impact of hydrodynamic conditions on performing the inhibitors was also conducted. The B3LYP (Becke, 3-parameter, Lee–Yang–Parr), HF (Hartree–Fock), M062X approach with 6–31++*G*(d,p) basis sets was employed using the Gaussian software to study the inhibitory activities of molecules in the gas and water phases.

Significant findings: According to the PDP test, there is a direct correlation between the amount of inhibitor and resistance to corrosion in static conditions, where the reduced ligand was more efficient. The EIS data revealed that, in a 1.0 M HCl solution with an inhibitor concentration of 250 ppm, the ligand and its reduced form enhanced corrosion resistance by 86.38% and 91.43%. Furthermore, these values were found to be 33.46% and 57.77%, in turbulent environment of 500 rpm. The atomic force microscopy (AFM) studies revealed that the ligand and its reduced form decreased surface roughness by 13.61% and 85.37% in static conditions and 59.67% and 61.53% in a hydrodynamic environment in comparison to 1.0 M HCl solution. Additionally, the UV test demonstrated that the amounts of iron corrosion was less severe in $H2L^2$ than in $H2L^1$ and 1.0 M HCl. Under static and dynamic conditions, the samples had lower specific weight changes during the immersion test, indicating that the inhibitory chemicals protected the samples' surfaces. Both compounds followed the Langmuir adsorption process. Furthermore, quantum chemical parameters simulations indicate the compounds' anti-corrosive abilities.

1. Introduction

In the past several decades, plain carbon steels have become the most widely used engineering alloys because of their high strength, low price, and uncomplicated weldability [1,2]. Some of the essential applications of mild steel are oil and gas transmission lines, the construction of tankers, and the automobile industry [3–5]. Unfortunately, despite all the superior features of plain carbon steels, these alloys are weak against corrosive environments [6]. For example, Dia et al. [7] reported that in the US, UK, China, and the EU, 25% of oil transmission lines fail, and 18% of gas transmission accidents are caused by corrosion damage. In recent years, accidents caused by the leakage of materials into the environment caused by pitting corrosion have increased as the pipes aged over time [8].

One of the essential corrosion factors in mild steels is an acidic medium. Notably, hydrochloric is one of the industrial and academic acids used to clean surfaces or investigate the corrosion resistance of alloys [9, 10]. Because of this, researchers have often been intrigued by the use of various chemical compounds to reduce corrosion [11–13]. For example, Aldehydes and Amines are essential commercial corrosion inhibitors [14]. Polymeric compounds are also used as well [15]. Natural inhibitors are well-known compounds due to their biocompatibility.

* Corresponding authors.
E-mail addresses: s.karimi@hut.ac.ir (S. Karimi), mrezaeivala@hut.ac.ir (M. Rezaeivala).

https://doi.org/10.1016/j.jtice.2023.104937
Received 3 March 2023; Received in revised form 5 May 2023; Accepted 23 May 2023
Available online 31 May 2023
1876-1070/© 2023 Taiwan Institute of Chemical Engineers. Published by Elsevier B.V. All rights reserved.

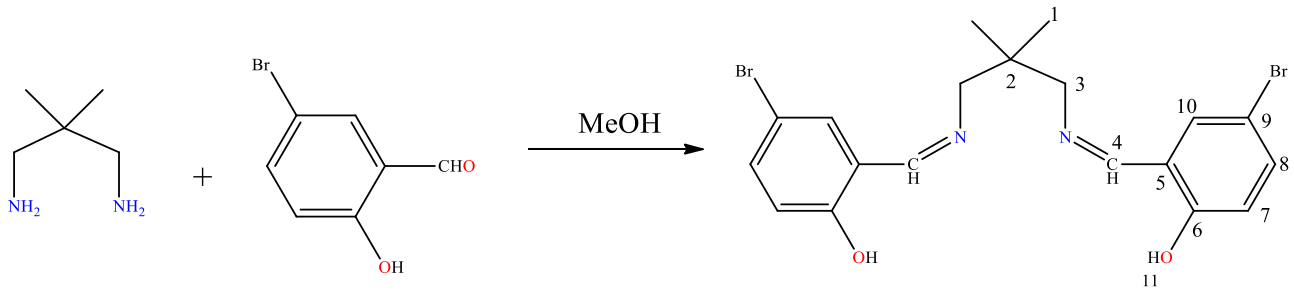

Fig. 1. Synthesis of 2,2′-((1Z,1′Z)-((2,2-dimethylpropane-1,3-diyl)bis(azanylylidene))bis(methanylylidene))bis(4-bromophenol)) ($H2L^1$).

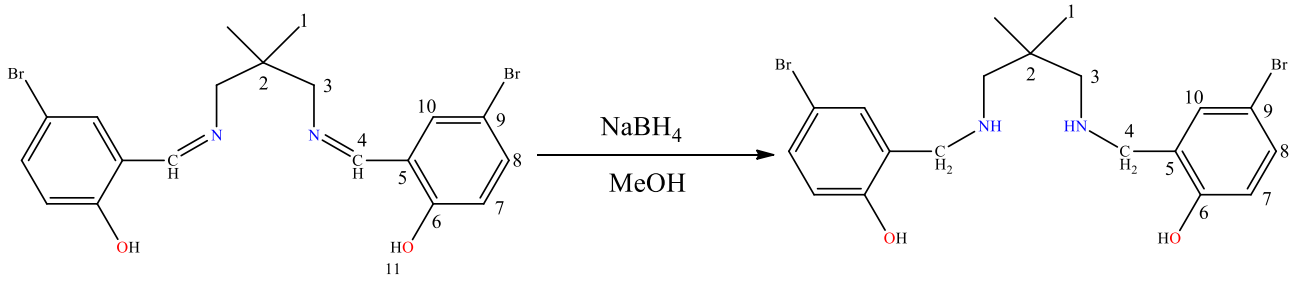

Fig. 2. Synthesis of 2,2′-(((2,2-dimethylpropane-1,3-diyl)bis(azanediyl))bis(methylene))bis(4-bromophenol) ($H2L^2$).

According to researchers, organic compounds extracted from plants like Rollinai [16], Fics Tikoua [17], Alba pendula [18], Musa paradisiaca [19], Azadira indica [20], and Dardagan Fruit [21] can successfully reduce the corrosion rate of plain carbon steel as an inhibitor. What is more, according to the reports, the compounds like 5(chloromethyl) 8quino-hydrochloride with 97% efficiency [22], 1-(4-methyl phenyl)−1H-Pyrrole-2,5dine with 97.5% efficiency [23], pyran [24,25], and 8-hydroxyquinoline with >90.0% efficiency [26,27] can prevent corrosion of mild steel in acidic media.

Unfortunately, one primary problem with organic inhibitors is their high price and toxicity to humans; therefore, their widespread use in the industry faces serious problems [28,29]. For this reason, synthetic organic inhibitors have attracted more attention because of their high inhibition efficiency, low price, and uncomplicated solubility in water, which are recently also becoming more environmentally friendly [30].

According to Hegazi et al. [31], Schiff bases are better inhibitors than Amides and Aldehydes, effectively reducing the corrosion rate on all steel, aluminum, and copper alloys. In previous works, we have prepared some Schiff base ligands with various applications, such as antibacterial [32,33], antifungal [34], DNA binding [33], anticancer [35,36], chemosensor [37] and anti-corrosion [38–41].

Due to their aldehyde rings and imine bond (-C = N-), Schiff bases tend to stick on the steel surface through the pair of electrons of the π layer with d electron layers of iron. The steel surface develops a thin film as a result of these electron-donating groups, which also reduces the corrosion's active zones. Therefore, the corrosion rate will decrease in both anodic and cathodic reactions in the HCl acid environment. Furthermore, adding halogens to the Schiff base composition will increase the inhibition efficiency because of the increase in electron density [42–46]. There are various substitutes for organic compounds in Schiff bases; for example, $-NO_2$, $-CH_3$, and $-Br^-$ are the most effective alternates due to their higher electron donation ability, which improves the inhibition and the substrate physical connection [47]. In non-metallic Schiff bases, the Br group has numerous applications in catalysts due to their particular surface properties [48]. Br-containing Schiff bases also prevent corrosion in HCl media [49]. In addition, these compounds protect the steel surface against corrosive media, especially in acidic environments [50].

This work investigated a new synthetic Br-containing Schiff base ($H2L^1$) and its related reduced form ($H2L^2$). The tests were performed in static and hydrodynamic conditions for a more detailed investigation. Atomic force microscopy (AFM) investigations of the samples were also conducted for corrosion surface morphology. Theoretical calculations are a standard method used to explain many chemical properties of the protonated form of the molecules [51]. Calculations are made for some quantum chemical descriptors. Three alternative methods— B3LYP (Becke, 3-parameter, Lee–Yang–Parr), HF (Hartree–Fock), and M062X—with a 6–31++*G*(d,p) basis set are used in these calculations with the help of the Gaussian package program.

2. Experimental

We prepared 5-bromo-2-hydroxybenzaldehyde and 2,2-dimethlpropane-1,3-diamine from Aldrich and Merck Company, respectively. Fourier transform infrared (FT-IR) spectra of KBr discs were measured on a BIO-RAD FTS-40A spectrophotometer (4000–400 cm^{-1}). ^1H and ^{13}CNMR spectra were determined using a Bruker 500 spectrometer in $CDCl_3$ at room temperature. Tetramethyl Silan served as the internal standard. The elemental analysis were measured using a Perkin-Elmer model 2400 analyzer (C, H, N, S, and O).

2.1. Synthesis

2.1.1. 2,2′-((1Z,1′Z)-((2,2-dimethylpropane-1,3-diyl)bis(azanylylidene)) bis(methanylylidene)) bis(4-bromophenol) synthesis ($H2L^1$)

The inhibitor ($H2L^1$) was created following methods described in the literature [41]. A stirred solution of 5-bromo-2-hydroxybenzaldehyde (1.0 mmol, 0.201 g) in methanol was added drop-wise to a solution of 2, 2-dimethlpropane-1,3-diamine (0.051 g, 0.5 mmol) in 20 mL of methanol (30 mL). The mixture was refluxed after stirring for 12 h. The progress of reaction was checked by TLC. The product was filtered off, washed with cold ethanol, and dried in vacuo. Yield: (85%). Anal. Calc. for $C_{19}H_{20}Br_2N_2O_2$: C, 48.74; H, 4.31; N, 5.98. Found: C, 48.89; H, 4.23; N, 6.22%. IR (KBr, cm^{-1}): 1630 υ(C = N), 1603, 1477 υ(C = C). ^1H NMR ($CDCl_3$, ppm) δ=1.09 (s, 6H, H-1); 3.52 (s, 2H, H-3); 6.89 (d, 1H, H-8); 7.41 (s, 1H, H-9); 7.45 (d, 1H, H-10); 8.30(s, 1H, H-4); 13.55 (s, 1H, H-11). ^{13}C NMR ($CDCl_3$, ppm) δ=24.35 (c-1); 36.31 (c-2); 68.11 (c-3); 101.34 (c-9); 119.03 (c-7); 120.02 (c-5); 133.49 (c-10); 135.07 (c-8);

160.27 (c-4); 164.61 (c-6) (Fig. 1). EI-MS calcd 468.18, Found: 468.34 $[H2L^1]^+$.

2.1.2. 2,2′-(((2,2-dimethylpropane-1,3-diyl)bis(azanediyl))bis (methylene))bis(4-bromophenol) ($H2L^2$)

The inhibitor ($H2L^2$) was prepared using the literature methods [38]. To a methanolic solution of 2,2′-((1Z, 1′Z)-((2,2-dimethylpropane-1, 3-diyl)bis(azanylylidene))bis (methany- lylidene))bis(4-bromophenol) (0.936 g, 2 mmol), excess $NaBH_4$ (0.76 g, 20 mmol) was added carefully in substantial incremental amounts with stirring. The mixture was stirred for 24 h before filtering and drying the concentrated solution at low pressure. The progress of reaction was checked by TLC.Yield: 70%. —Anal. Calc. for $C_{19}H_{24}Br_2N_2O_2$: C: 48.33; H, 5.12; N, 5.93. Found: C, 48.55; H, 5.03; N, 617%. IR (ATR, cm^{-1}): 3308(υ N-H), 1610, 1578, 1480 (υC=C). ^1H NMR ($CDCl_3$, ppm): δ=1.10 (s, 6H, H-1), 2.50 (s, 4H, H-3), 3.94 (s,4H, H-4), 6.71 (d, 2H, H-7), 7.13 (d, 2H, H-8), 7.24-7.27 (dd, 2H, H-10). ^{13}C NMR ($CDCl_3$, ppm): δ 24.32 (c-1), 34.49 (c-2), 52.71 (c-3), 57.23 (c-4), 131.13 (c-5), 131.58 (c-6), 110.87 (c-7), 138.35 (c-8), 124.40 (c-9), 157.11 (c-10) (Fig. 2). EI-MS: calcd 471.21, Found: 471.65 $[H_2L^2]^+$.

2.2. Measures of immersion times

The samples were trimmed to a size of 1 × 1 × 1 cm^3 for immersion measurements. The electrodes were then polished using emery paper measuring 1500#, cleaned with ethanol, and dried with a blow dryer. The samples were submerged for 12 h at room temperature in a particular volume of inhibitor-containing and inhibitor-free solutions. Then, the sample was taken out each hour, distilled water and ethanol were used to wash numerous times and then dried. Finally, the mass of the pieces was measured using a 4-decimal balance.

2.3. Calculation method

The chemical and biological properties of molecules can be learned from theoretical calculations [52]. Theoretical computations are used to determine the number of quantum chemical characteristics. The estimated parameters are employed to explain the molecules' chemical behaviors. Molecule calculations are done using a variety of programs. These programs are Gaussian09 RevD.01 and GaussView 6.0 [53,54]. Using these programs, B3LYP, HF, and M06–2x [55–57] methods were calculated using the 6–31++G(d,p) basis set in the gas and water phase. Many quantum chemical parameters have been discovered as a result of these studies. Each parameter describes a particular molecule's chemical characteristics. These factors include chemical potential, electrophilicity, chemical hardness, global softness, HOMO (Highest Occupied Molecular Orbital), and LUMO (Lowest Unoccupied Molecular Orbital). Other parameters include nucleophilicity, dipole moment, and energy value [58]. The following formula (Eq. (1)) could be used to calculate the theorical calculation.

$$\chi = -\left(\frac{\partial E}{\partial N}\right)_{\nu(r)} = \frac{1}{2}(I+A) \cong -\frac{1}{2}(E_{HOMO}+E_{LUMO})$$
$$\eta = -\left(\frac{\partial^2 E}{\partial N^2}\right)_{\nu(r)} = \frac{1}{2}(I-A) \cong -\frac{1}{2}(E_{HOMO}-E_{LUMO})$$
$$\sigma = \frac{1}{\eta} \quad (1)$$
$$\omega = \frac{\chi^2}{2\eta}$$
$$\varepsilon = \frac{1}{\omega}$$

2.4. Preparation of electrodes and solution

The carbon steel's chemical makeup is as follows: 0.05 wt.% C, 0.22 wt.% Mn, 0.01 wt.% Si, 0.01 wt.%P and Fe balance were used as a working electrode (WE) to investigate the corrosion performance of inhibitors. The WEs were divided into 1 × 1 × 1 cm^3 pieces, and their five surfaces were subsequently varnished so that just 1 × 1 cm^2 of surface area was accessible to the electrolyte. The WEs were consistently polished with 600# to 2000# emery paper before each test, washed with distilled water and ethanol, and dried with a blow dryer. The corrosion solution, which included 1.0 M HCl, was created by combining distilled water with analytical grade (37%) HCl. Two inhibitors, $H2L^1$ and $H2L^2$, were added to the corrosion solution to prepare corrosion solutions with ligand concentrations of 0 ppm, 50 ppm, 100 ppm, and 250 ppm.

2.5. Electrochemical experiments

The electrochemical impedance spectroscopy (EIS) experiments were carried out using a potentiostat/galvanostat set (Iviumstat compact 20,250 H) controlled by Ivium soft electrochemistry software, while the potentiodynamic tests were carried out using a GSTAT101N potentiostat (Metrohm Autolab) controlled by Nova software (Version 2.1.4). A three-electrode system comprised of a working electrode (WE: carbon steel), a reference electrode (Ag/AgCl), and an auxiliary electrode was used to conduct corrosion tests at ambient pressure and without stirring (platinum).

At the start of each test, the WEs were immersed for 30 min in the solution with and without inhibitor to stabilize the open circuit potential (OCP). The potentiodynamic potential range was ±0.70 V vs. OCP, and the scan rate was a constant of 1 mV/s. EIS tests were conducted at OCP with a 10^{-1}–10^5 Hz frequency range and perturbation alternating voltage of 10 mV. The Nyquist diagram was fitted with Zsim software. For the electrochemical measurements, the values of standard deviation are lower than 3.3%, which demonstrates relatively excellent reproducibility of the electrochemical experiments. The calculated charge transfer resistance (R_{ct}) was used to measure the inhibition efficiency (η) of the inhibitors by the Eq. (2):

$$\eta(\%) = \frac{R_{ct} - R_{ct}^0}{R_{ct}} \times 100 \quad (2)$$

Where R_{ct} and R_{ct}^0 represent the carbon steel's charge transfer resistance with and without inhibitors, respectively.

2.6. Surface characterization

The surface morphology of carbon steel was examined using atomic force microscopy (AFM) after 12 h of immersion in 1.0 M HCl with and without an inhibitor at room temperature. Using spring constants of 20–80 N/m at 5 m, the AFM analysis was carried out using a BRISK atomic force microscope (ARA Research) at 335–363 kHz.

2.7. Examination of ultraviolet-visible (UV) spectroscopy

To evaluate the components dissolved in HCl media, the samples were immersed in each solution for 10 days and then the Bell (BEL UV-M51) machine was used to conduct a UV spectrum test.

3. Result and discussion

3.1. Characterization of $H2L^1$ and $H2L^2$

3.1.1. FT-IR spectra

A Schiff base ligand ($H2L^1$) was created by condensing 2,2-dimethlpropane-1,3-diamine and 5-bromo-2-hydroxybenzaldehyde in

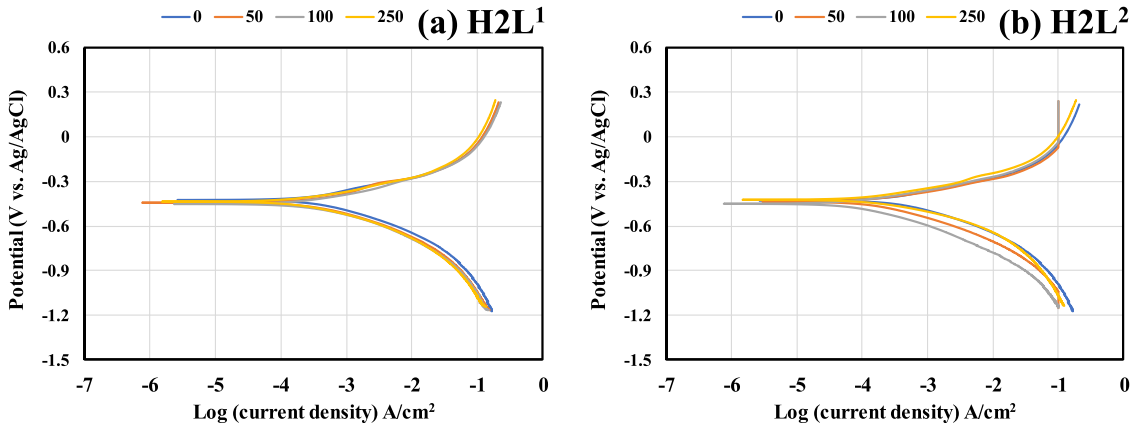

Fig. 3. PDP diagram for carbon steel in the absence of various concentrations of (a) $H2L^1$ and (b) $H2L^2$ inhibitors in 1.0 M HCl static solution.

Table 1
Carbon-steel PDP diagram data that was extracted in the absence of various concentrations of $H2L^1$ and $H2L^2$ inhibitors in 1.0 M HCl solution.

Sample	*Conc.* (ppm)	E_{corr} (mV)	i_{corr} (A/cm^2)× 10^{-4}	β_a (V/dec)	$-\beta_c$ (V/dec)
HCl 1.0 M	0	−418	7.94	0.39	0.25
$H2L^1$	50	−422	4.68	0.28	0.16
	100	−440	3.89	0.21	0.17
	250	−442	3.09	0.20	0.17
$H2L^2$	50	−422	3.31	0.16	0.15
	100	−444	3.23	0.17	0.16
	250	−446	3.02	0.18	0.15

methanol for six hours in a 1:2 molar ratio. The generated Schiff base was characterized using microanalysis and a number of spectroscopic techniques. The sharp band at 1630 cm^{-1} in the FT-IR spectra of the Schiff base ligand, which is associated with the stretching vibration frequency of the mine group, is indicative of the condensation of the precursors to produce the Schiff base ligand.

3.1.2. NMR spectral studies

The ^{1}H and ^{13}C NMR spectra of the compounds were recorded in $CDCl_3$. The peaks obtained were consistent with the structures of the synthesized compounds. The imino proton of ligand was observed at 8.30 ppm. The ^{13}C NMR spectrum showed the signals due the aromatic carbons which appeared in the range 101.34-164.61 ppm. The signal due to the imino carbon of the $H2L^1$ appeared at 160.27 ppm.

3.2. Electrochemical measurements in 1.0 M HCl

3.2.1. Potentiodynamic polarization

The potentiodynamic polarization (PDP) measurements of carbon-steel in corrosion solution with and without inhibitors are presented in Fig. 3. The deduced corrosion parameters from the PDP diagram, including corrosion current density (i_{corr}), corrosion potential (E_{corr}), PDP slopes (β_a and β_c) are illustrated in Table 1. Overall, the form of the PDP curve of the carbon-steel immersed in 1.0 M HCl (inhibitor-free) does not alter reasonably in comparison with the PDP curves with inhibitors $H2L^1$ and $H2L^2$, suggesting no reasonable variation in the polarization resulting between with and without inhibitors solutions. The i_{corr} of carbon steel in the inhibitor-containing solution also drops significantly simultaneously. The results showed that adding two inhibitors did not alter the reactions on the metal's surface but that it did

Table 2
EIS specifications for a comparable circuit of Fig. 4.

Inhibitor type	Concentration (ppm)	R_{ct} (Ω cm^2)	Q_{dl}		χ^2	η (%)
			Y_0 (Ω s^{-n})	n		
HCl 1M	–	44.38	1.032×10^{-3}	0.83	0.009	–
$H2L^1$	50	176.5	3.076×10^{-4}	0.74	0.009	74.85
	100	273.1	1.936×10^{-4}	0.78	0.007	83.75
	250	325.8	2.252×10^{-4}	0.77	0.006	86.38
$H2L^2$	50	279.2	2.521×10^{-4}	0.76	0.003	84.10
	100	436.3	2.310×10^{-4}	0.78	0.007	89.82
	250	517.9	2.302×10^{-5}	0.72	0.004	91.43

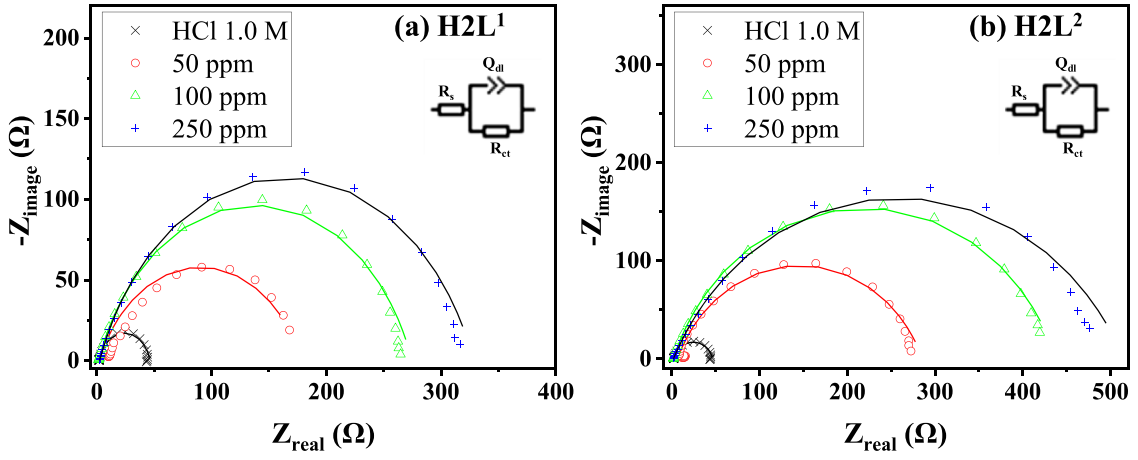

Fig. 4. Nyquist diagram of carbon steel at OCP in free and inhibitor-containing solution was measured and simulated.

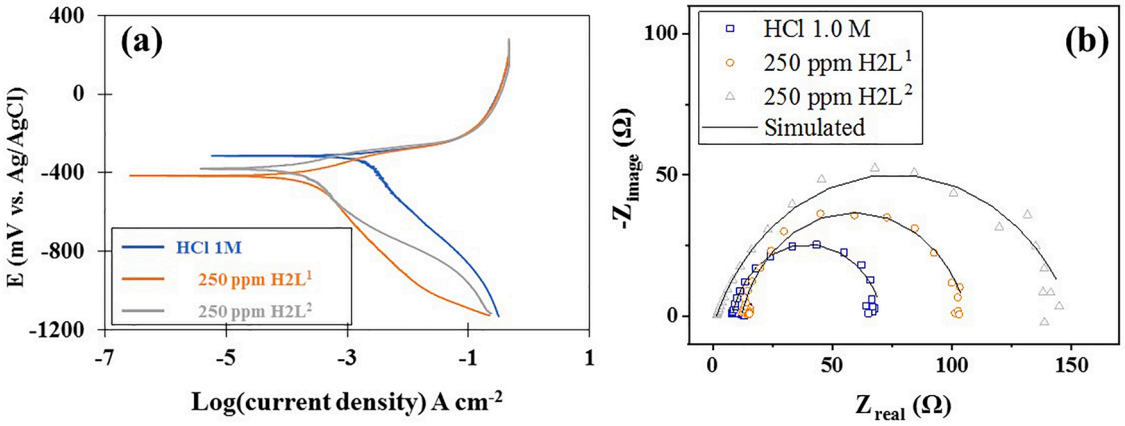

Fig. 5. Simulated and measured Nyquist impedance spectra of carbon-steel at OCP in 1.0 M HCl, $H2L^1$, and $H2L^2$ solutions with a concentration of 250 ppm under hydrodynamic electrolyte conditions with an intensity of 500 rpm.

Table 3
PDP diagram information for carbon steel in solutions containing 250 ppm inhibitors and 1.0 M HCl under hydrodynamic conditions.

Type solution	HCl 1.0 M	250 ppm $H2L^1$	250 ppm $H2L^2$
i_{corr}	19.95×10^{-4}	2.40×10^{-4}	1.74×10^{-4}
E_{corr}	−308	−395	−350

Table 4
EIS specifications for a comparable circuit of Fig. 5.

Inhibitor type	R_{ct} (Ω cm^2)	Q_{dl}		χ^2	η (%)
		Y_0 (Ω s^{-n})	n		
HCl 1M	62.8	5.592×10^{-4}	0.87	0.001	–
$H2L^1$ (250 ppm)	94.4	4.734×10^{-4}	0.84	0.002	33.46
$H2L^2$ (250 ppm)	148.7	3.548×10^{-4}	0.75	0.003	57.77

slightly slow down the cathodic hydrogen evolution reaction (HER) and the anodic dissolution of carbon-steel, which reduced the rate of corrosion reactions on both the cathodic and anodic sites [59]. For example, the i_{corr} of the carbon-steel in inhibitor-free (1.0 M HCl) is 7.94×10^{-4} A/cm^2 demonstrating a considerably decreasing to 3.09×10^{-4} A/cm^2 for inhibitor $H2L^1$ and 3.02×10^{-4} A/cm^2 for inhibitor $H2L^2$. The highest i_{corr} value proves the fastest corrosion rate in metal electrodes [60]. The lower i_{corr} value for inhibitor-containing solutions may result from forming a protective layer with an inorganic component on the metal's surface [61]. The same result has been reported by Rbaa et al. [62,63], in which there is a reduction in i_{corr} by increasing the inhibitor concentration. The i_{corr} value for carbon steel in the presence of $H2L^1$ is reduced from 4.68×10^{-4} to 3.09×10^{-4} A/cm^2 as the corrosion inhibitor concentration increases from 50 to 250 ppm. The same trend can be seen for inhibitor $H2L^2$, in which the PDP curves were shifted towards lower i_{corr} by the increment of inhibitor between 50 and 250 ppm. This shift is more evident with the rise in the inhibitor concentration relative to the inhibitor-free solution (1.0 M HCl) [52,58].

As seen in Table 1, $H2L^2$ has a lower i_{corr} than $H2L^1$ at the same concentration. The corrosion inhibition of a reduced form of Schiff base compound has been studied by Emregul and Atakol [64] in 1.0 M HCl. The findings demonstrated that the strength of the adsorption process might be controlled by the electrons of the imine group [64,65]. In addition, the imine group (-C = N-) in Schiff base molecules causes a higher inhibition efficiency in the acidic solution [58]. The reduced form of the $H2L^2$ molecules does not hydrolyze in acidic media because of the high stability of the amine bond (−C−NH) [66].

By Assessing Table 1, in all solutions, β_a and β_c values decrease with the addition of the inhibitors relative to the inhibitor-free solution. The cathodic and anodic slopes show that the two inhibitors' addition to 1.0 M hydrochloric acid decreases the cathodic and anodic reactions (HER and anodic dissolution). The variation in E_{corr} values between solutions with and without inhibitors was less than 85 mV, indicating that the

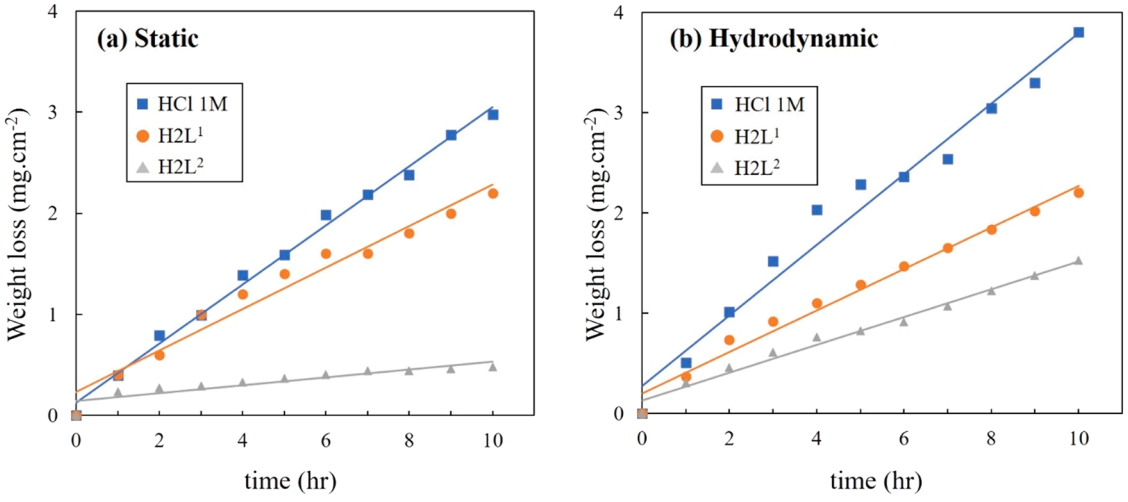

Fig. 6. Corrosion rate of carbon steel under static and hydrodynamic conditions and in the presence and absence of 250 ppm of $H2L^1$ and $H2L^2$ inhibitor.

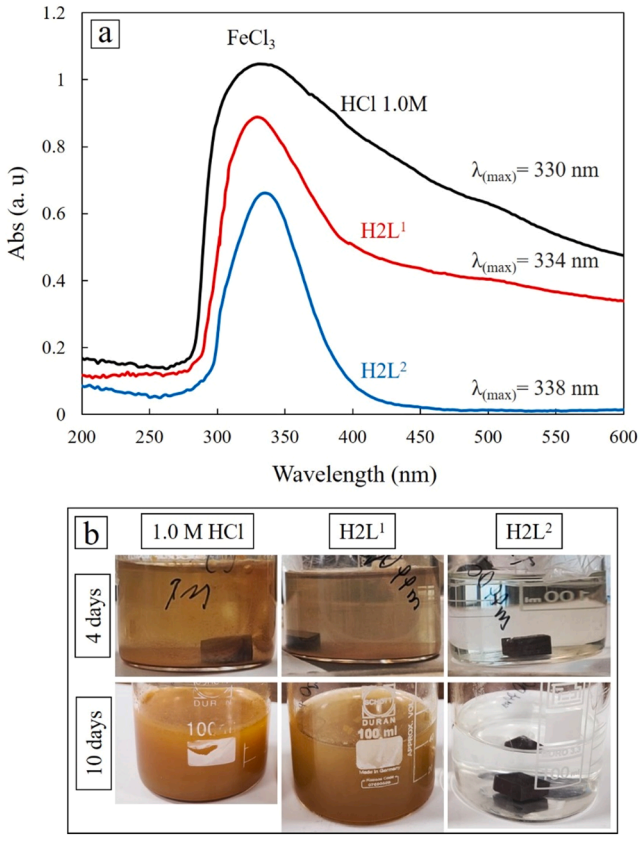

Fig. 7. (a): The UV spectra of the solutions comprising 1.0 HCl, 250 ppm $H2L^1$, and $H2L^2$ following ten days of submersion. (b): Images of specimens after 4 and 10 days.

inhibition mechanism follows mixed-type behavior [67]. As stated in previously published papers, the rate of anodic and cathodic reactions was equal on the metallic surface [68].

3.2.2. EIS evaluation

The EIS of carbon steel acting as the working electrode in 1.0 M hydrochloric acid solution with and without inhibitors at room temperature is recorded to examine the two inhibitors' inhibition performance further. The interface behavior of carbon steel and solution can be studied using the EIS experiment. Whether or not inhibitors are present, the Nyquist impedance spectra of carbon steel at the OCP exhibit the same patterns, as illustrated in Fig. 4. (a single depressed loop in the testing frequency range). Their depressed loop corresponds to the roughness and inhomogeneity of the carbon-steel surface and thin film paper [69]. The impedance morphologies of carbon steel do not differ when inhibitors are present or absent, indicating that the corrosion mechanism is unaffected by the 1.0 M HCl solution [70]. The diameter of capacitive semicircles enlarged with an increment of the inhibitor concentration, indicating that $H2L^1$ and $H2L^2$ slow down the charge transfer process at the carbon-steel/solution interface, thus diminishing the metal corrosion in the 1.0 M HCl solution. This response supports the hypothesis that a protective coating has formed on the metal surface due to the increasing concentration of $H2L^1$ and $H2L^2$ inhibitors in an acidic solution.

A solution resistance ($R_{sol.}$) in series with a constant phase element/charge transfer resistance (Q_{dl}/R_{ct}) is chosen as the corresponding electrical circuit to fit the EIS data. The electrochemical data are tabulated in Table 2. The R_{ct} value for carbon steel without an inhibitor is 44.38 Ω cm^2, the lowest compared with the charge transfer resistance in inhibitor-containing solutions. From Table 2, the R_{ct} for carbon steel in the presence of $H2L^1$ was 176.5, 273.1, and 325.8 Ω cm^2 for inhibitor concentrations of 50, 100, and 250 ppm, respectively. The charge transfer resistance value for the $H2L^2$ inhibitor follows the sequence 250 ppm > 100 ppm > 50 ppm, demonstrating a similar pattern. As is already known, the R_{ct} values and inhibition efficiency are strongly correlated, meaning that corrosion resistance increases with increasing charge transfer resistance. It is apparent from Table 2 data that the inhibition performance of $H2L^2$-containing solutions is much better than $H2L^1$ solutions because of the higher R_{ct} value at the same inhibitor concentration.

The EIS results follow the PDP data. In an HCl solution, carbon steel exhibits the least corrosion resistance. As shown in PDP curves, the inhibition performance inhibitors $H2L^1$ and $H2L^2$ increase in the range of 50 to 250 ppm in hydrochloric acid solution, indicating that the protective film on the surface is prone to be compact at higher concentrations of inhibitors. Therefore, both EIS and PDP measurements show that carbon steel has the lowest corrosion rate in 250 ppm $H2L^2$ inhibitor, among other concentrations, thanks to its higher charge transfer resistance.

As known, replacing the inhibitor compound with H_2O and HCl molecules on the carbon steel provides anti-corrosion properties. Consequently, increased amounts of molecules that combat corrosion can be found in higher concentrations of inhibitors, and greater inhibition efficiency is provided due to the thicker protective coating and surface area coverage of the inhibitor [58,71]. According to the FT-IR data, this could be due to their inherent characteristic in nitrogen functional groups, which donor their electron when they reach the electrode surface [66]. The aromatic rings and hetero elements in amino acids structure increase the inhibition efficiency [72].

The inhibition efficiency (η) obtained from the R_{ct} is determined by Eq. (1), and their values are listed in Table 2. The η values for $H2L^1$ are 75.85, 83.75, and 86.38%, showing that as concentration increases, the reduction of hydrogen ions and anodic dissolution decrease by adsorbing more inhibitor molecules on the active sites. In comparison, carbon steel shows higher η in $H2L^2$-containing solutions. For instance, the 250 ppm concentration of $H2L^2$ exhibited 91.43% inhibition efficiency, while at the exact dosage for $H2L^1$, η decreased by about 4%. Conclusion: The $H2L^2$ showed amazing inhibitory effectiveness in a hydrochloric acid environment. Most likely, Because the $H2L^1$ inhibitor is less stable in 1.0 M HCl solution than the $H2L^2$ inhibitor, there is a difference in η between these two inhibitors.

3.3. Electrochemical in hydrodynamic electrolyte

Fig. 5a shows the Tafel test results for the samples tested in 1.0 M HCl, $H2L^1$, and $H2L^2$ solutions with a concentration of 250 ppm under hydrodynamic electrolyte conditions with an intensity of 500 rpm. Fig. 5b also indicates the EIS test results and the simulated curves. In addition, the parameters extracted from the Tafel curve (i_{corr} and E_{corr}) and the variables extracted from the EIS curve were reported in Tables 3 and 4, respectively.

As can be observed, in all situations, the corrosion rate of carbon steel in solution without an inhibitor is the highest. Adding an inhibitor to the HCl solution has significantly reduced the corrosion current, and this value is the lowest in the $H2L^2$ solution. Also, adding an inhibitor to the hydrodynamic acid solution has increased the corrosion potential.

The transfer resistance values of the EIS test also confirm the PDP test results, so that the R_{ct} is higher in solutions with inhibitors, which is the maximum value for solution $H2L^2$ solution. According to the results, the inhibition efficiency of the $H2L^1$ solution equals 33.46%, and for $H2L^2$ is 57.77% in the hydrodynamic flow.

One of the essential effects of hydrodynamic corrosion conditions is preventing the formation of a protective film and hydrogen bubble detachment [73]. So, the turbulence will cause a significant increase in the corrosion rate compared to static conditions, as confirmed by the i_{corr} values of the Tafel test. Also, in an HCl acidic environment, the hydrodynamic flow will cause more H^+ and Cl^- ions movement; thus, the

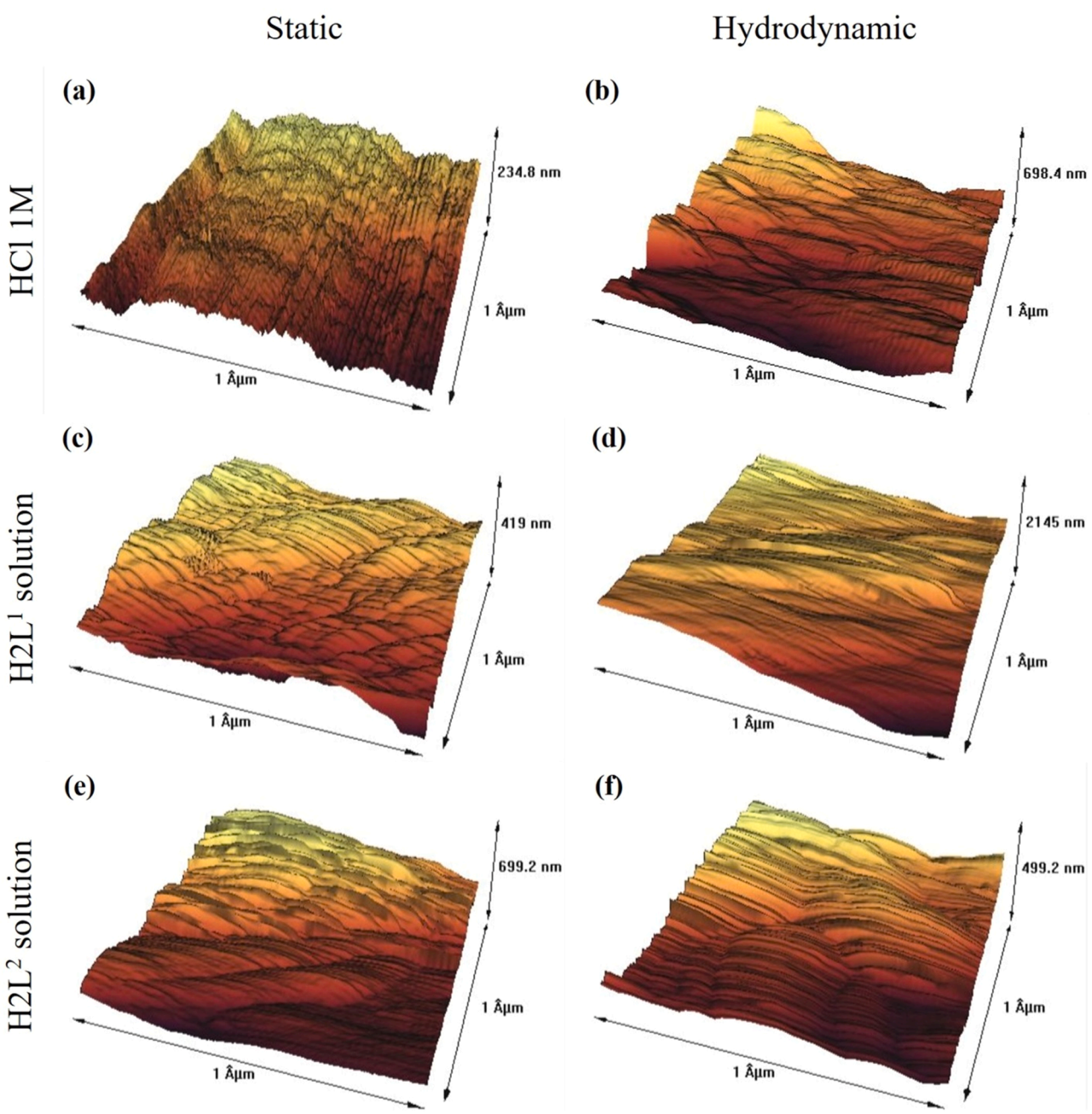

Fig. 8. The AFM three-dimensional optical images of immersed samples at static and hydrodynamic electrolytes at 1.0 M HCl, 250 ppm of $H2L^1$ and $H2L^2$.

conditions will become more corrosive [74]. Despite all the harmful effects of turbulence electrolyte flow, hydrodynamic conditions will cause more movement of inhibitory molecules. In contrast, it also stresses surface shear force, affecting corrosion efficiency [75]. The significant finding is the synergistic relationship between surface roughness and corrosion rate, which means that in a hydrodynamic flow, a rough surface corrodes more [76]. Given the smoothness of our samples' surfaces (#2000 sandpaper mesh), it appears that the $H2L^2$ solution provides higher corrosion resistance because the inhibitor molecules adhere to the surface more effectively.

3.4. Immersion time measurements

The corrosion rate (*CR*) of carbon steel was measured using the immersion method under static and hydrodynamic circumstances, both in the presence and absence of inhibitors $H2L^1$ and $H2L^2$ (as depicted in Fig. 6). Using this method shows the stability of inhibitors and anti-corrosion features on a time scale. The *CR* for carbon steel multiplies over time in static and hydrodynamic circumstances in an inhibitor-free solution, as illustrated in Fig. 6. The results show that adding an $H2L^1$ inhibitor to a 1.0 M HCl solution both in static and hydrodynamic effects in a reduction of *CR* for carbon steel, with the maximum *CR* corresponding to the carbon steel in the 1.0 M HCl solution (i.e., inhibitor-free solution). Of course, compared to an inhibitor-free condition, the *CR* reduction is more pronounced in the dynamic solution in the $H2L^1$-containing solution. Moreover, the *CR* for carbon steel in the $H2L^2$-containing solution drops significantly. Compared to 1.0 M HCl and $H2L^1$ solutions, the carbon steel in the $H2L^2$-containing solution will live longer and experience the lowest *CR*. Based on the slope of immersion tests, the *CR* values for inhibitor-free, $H2L^{1,}$ and $H2L^2$ solutions are 0.292, 0.205, and 0.038 $mg.cm^{-2}.h^{-1}$ in static conditions. However, in hydrodynamic solutions, the *CR* rate for all samples increased by 0.351

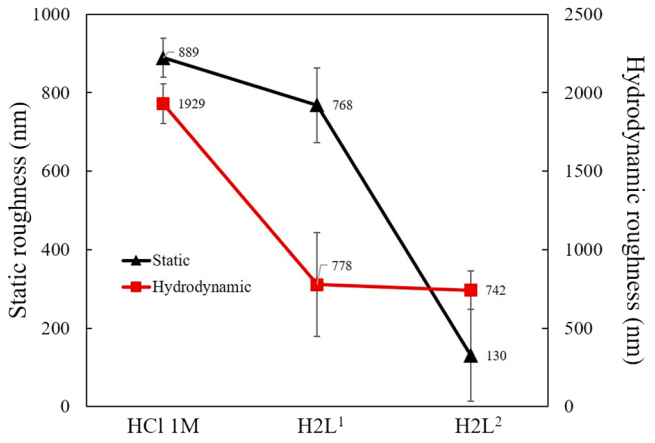

Fig. 9. Average surface roughness of samples extracted from AFM data.

mg.cm^{-2}.h^{-1} for 1.0 M HCl, 0.207 mg.cm^{-2}.h^{-1} for H2L^1 and 0.139 mg.cm^{-2}.h^{-1} for H2L^2 solutions. Previously published papers have reported similar results in static conditions [16,68]. The best that we can tell, no data exist on carbon steel's *CR* in hydrodynamic conditions.

3.5. UV spectroscopy

The graph in Fig. 7(a) depicts the UV absorption pattern of samples that were immersed in 1.0 M HCl and 250 ppm of H2L^1 and H2L^2 for 10 days, with the results being normalized with pure solutions. Monochromatic light absorption is a suitable technique for identifying complex ions, which has a direct correlation to the amount of absorbing material present. A distinct peak in the range of 290 to 380 nm is present in all three samples with varying intensities, which is associated with the composition of $FeCl_3$ [77]. The formation of iron chloride by hydrochloric acid follows Eq. (3):

$$Fe_{(s)}+3HCl_{(aq)} = FeCl_{3\ (aq)}+3/2H_{2\ (g)} \quad (3)$$

It is observable that the higher intensity is due to the acidic environment of 1.0 M HCl without the inhibitors. Fig. 7(b) also indicates the vigor of the reactions over time, nevertheless, in H2L^1 and H2H^2 solutions, the intensity of the reactions is less significant and a smaller amount of iron has been corroded proving the UV data. The H2L^2 solution demonstrated the least intensity of $FeCl_3$, and the alteration in the solution's color was minimal.

3.6. AFM characterization

One of the most valuable tools to investigate surface morphology and corrosion progress at the interface between steel and acid is using an AFM. Three-dimensional images taken from the surface area of 1 × 1 cm^2 for samples immersed in 1.0 M HCl, H2L^1, and H2L^2 solutions, which were in static and dynamic conditions for 10 h, are shown in Fig. 8. The average roughness number shown in Fig. 9 indicates the severe acid

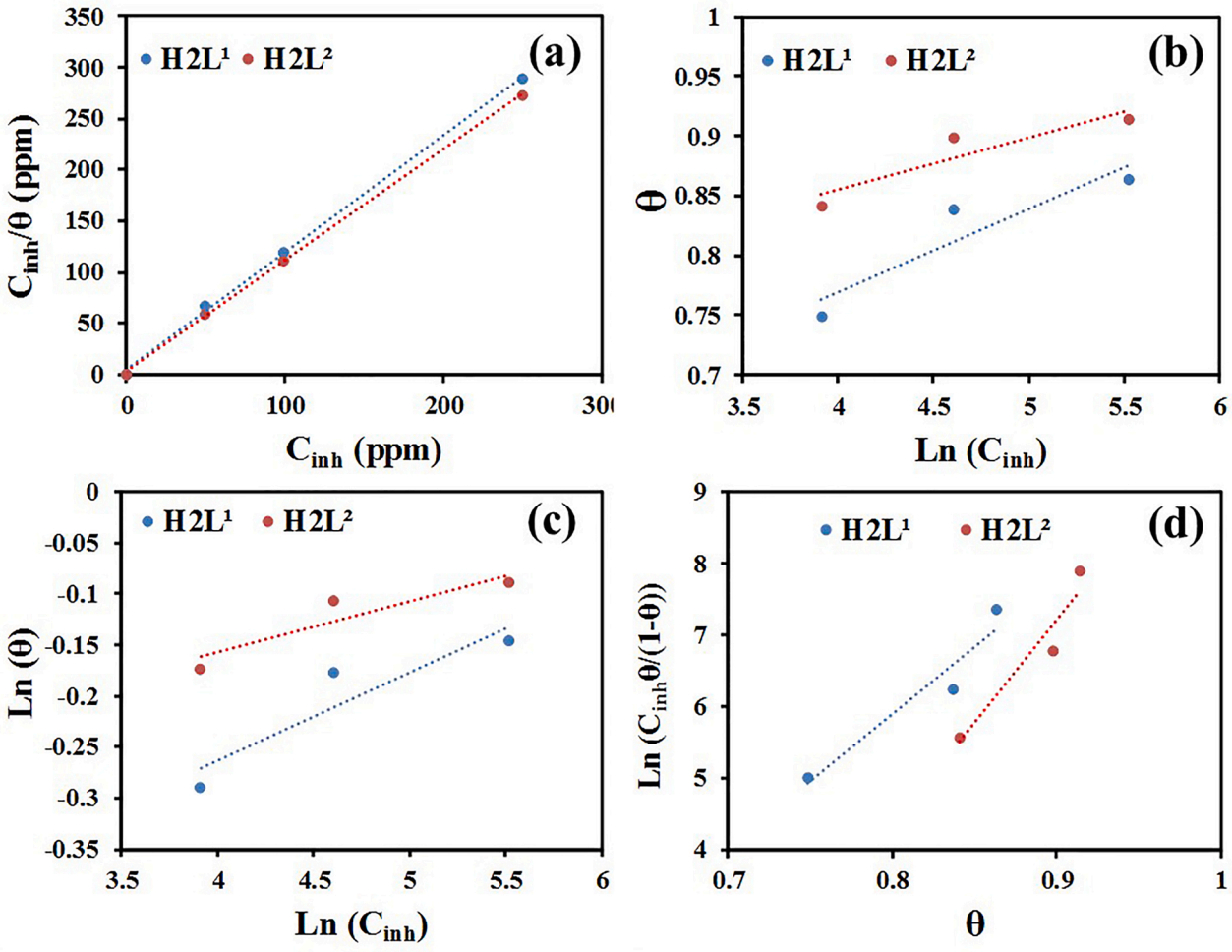

Fig. 10. Graphical representation of adsorption isotherms of H2L^1 and H2L^2 for carbon steel surface in 1.0 M HCl at 298 K (a) Langmuir, (b) Temkin, (c) Freundlich and (d) Frumkin.

Table 5
The isotherms parameters, ΔG^0_{ads} and $R^2$of Langmuir, Temkin, Freundlich and Frumkin models.

Model	R^2		a		K_{ads}		ΔG^0_{ads}(kJ/mol)	
	$H2L^1$	$H2L^2$	$H2L^1$	$H2L^2$	$H2L^1$	$H2L^2$	$H2L^1$	$H2L^2$
Langmuir	0.9997	0.9990	–	–	0.23	0.42	−11.98	−13.53
Temkin	0.8596	0.8527	−7.20	−11.33	1200.84	4,795,650.67	−27.52	−48.06
Freundlich	0.8506	0.8475	0.09	0.05	0.54	0.70	−8.44	−9.06
Frumkin	0.9261	0.9188	9.42	14.38	1.02×10^{-4}	7.62×10^{-9}	12.83	36.36

Table 6
The calculated quantum chemical parameters of protonated molecules.

	E_{HOMO}	E_{LUMO}	I	A	ΔE	η	μ	χ	$P\dot{I}$	ω	ε	dipol	Energy
B3LYP/6–31++*G*(d,p) level in gas													
1	−8.4424	−6.3525	8.442	6.3525	2.0899	1.0449	0.9570	7.3975	−7.3975	26.184	0.0382	10.617	−167,068.4950
2	−8.2957	−4.3375	8.295	4.3375	3.9582	1.9791	0.5053	6.3166	−6.3166	10.080	0.0992	7.800	−167,133.3871
HF/6–31++*G*(d,p) level in gas													
1	−10.7314	−2.5944	10.731	2.5944	8.1371	4.0685	0.2458	6.6629	−6.6629	5.455	0.1833	10.062	−167,060.5014
2	−10.5880	−1.7611	10.588	1.7611	8.8269	4.4134	0.2266	6.1746	−6.1746	4.319	0.2315	8.148	−166,861.1077
M062X/6–31++*g*(d,p) level in gas													
1	−9.7420	−5.4325	9.742	5.4325	4.3095	2.1548	0.4641	7.5873	−7.5873	13.358	0.0749	10.062	−167,060.5014
2	−9.6340	−3.4850	9.634	3.4850	6.1490	3.0745	0.3253	6.5595	−6.5595	6.997	0.1429	7.150	−167,125.2867
B3LYP/6–31++*G*(d,p) level in water													
1	−6.5188	−2.3840	6.518	2.3840	4.1348	2.0674	0.4837	4.4514	−4.4514	4.7923	0.2087	31.984	−167,068.3773
2	−6.3634	−1.3127	6.363	1.3127	5.0507	2.5254	0.3960	3.8381	−3.8381	2.9165	0.3429	11.234	−167,135.5391
HF/6–31++*G*(d,p) level in water													
1	−8.8364	0.9546	8.836	−0.9546	9.7910	4.8955	0.2043	3.9409	−3.9409	1.5862	0.6304	32.061	−166,798.5574
2	−8.7088	1.0362	8.708	−1.0362	9.7450	4.8725	0.2052	3.8363	−3.8363	1.5102	0.6622	11.254	−166,863.4052
M062X/6–31++*G*(d,p) level in water													
1	−7.8171	−1.4191	7.817	1.4191	6.3980	3.1990	0.3126	4.6181	−4.6181	3.3333	0.3000	31.737	−167,060.5432
2	−7.7028	−0.4210	7.702	0.4210	7.2818	3.6409	0.2747	4.0619	−4.0619	2.2658	0.4414	10.689	−167,127.4294

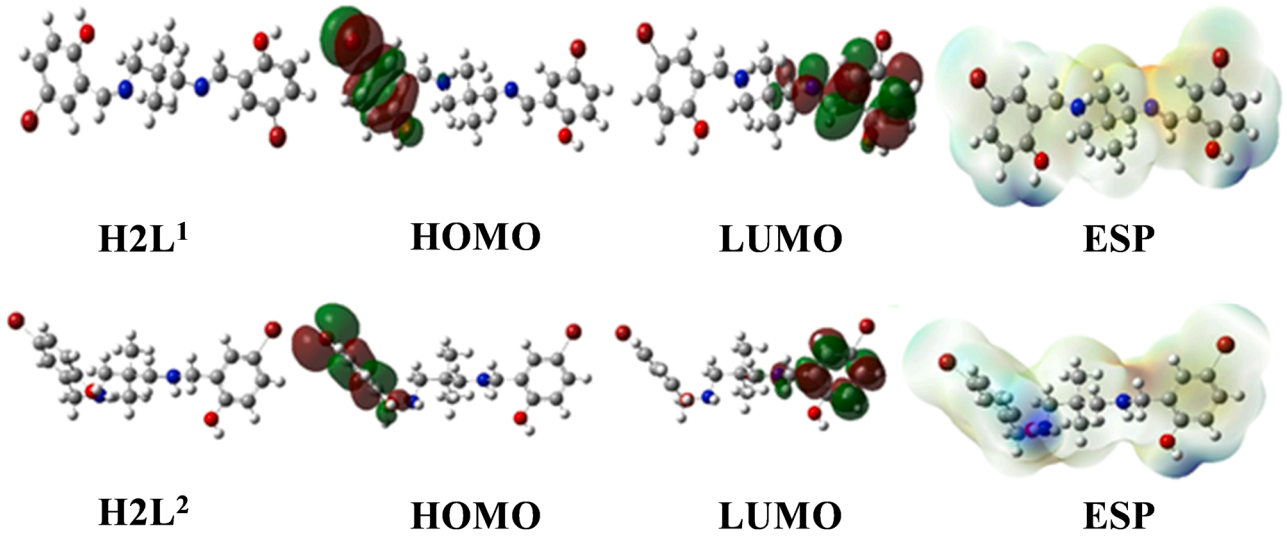

Fig. 11. HOMO, LUMO, and ESP representations of optimal structures.

attack on the steel surface in inhibitor-free samples. The results of the AFM analysis demonstrate that the steel surface in the inhibited samples is substantially smoother and denser, thereby implying a lower corrosion rate [78]. This surface smoothness is due to the adhesion of inhibitor molecules and corrosion prevention. In hydrodynamic conditions, the surface roughness of 1.0 M HCl indicates much more corrosive conditions with an increase of 216% than the static electrolyte. The $H2L^2$ performs better in dynamic and static modes due to the significant reduction in surface roughness. An interesting point is the absence of a sharp drop in surface roughness in the $H2L^1$-containing solution. Although this number is higher than $H2L^2$, this inhibitor may perform better in higher turbulences. In contrast, with an excellent agreement of electrochemical and EIS test results, $H2L^2$ is adequate for better performance, especially in static electrolyte conditions.

3.7. Adsorption mechanism

The adsorption mechanism of $H2L^1$ and $H2L^2$ at the interface between carbon-steel surface and 1.0 M HCl solution has been determined by evaluating the surface coverage at various inhibitor doses. The Langmuir, Temkin, Freundlich and Frumkin adsorption isotherms were calculated using the Eqs. (4)–(8) [79].

$$\text{Langmuir}: \frac{C_{inh}}{\theta} = \frac{1}{K_{ads}} + C_{inh} \tag{4}$$

Table 7
Fukui function value of $H2L^1$ molecule.

Atoms	$f+$	f⁻	f
1C	0.02	0.10	0.06
2C	0.01	0.01	0.01
3C	0.01	0.06	0.03
4C	0.02	0.08	0.05
5C	−0.02	−0.12	−0.07
6C	0.02	0.09	0.05
7H	0.04	0.10	0.07
8H	−0.01	0.10	0.05
9H	−0.06	0.09	0.02
10Br	0.10	0.22	0.16
11O	−0.04	0.01	−0.01
12H	0.04	0.03	0.04
13C	−0.11	0.04	−0.03
14H	0.11	0.03	0.07
15N	0.26	−0.03	0.12
16C	−0.26	0.18	−0.04
17H	0.09	0.03	0.06
18H	0.10	0.02	0.06
19C	−0.03	−0.01	−0.02
20C	−0.02	0.00	−0.01
21H	0.04	0.02	0.03
22H	−0.04	−0.03	−0.04
23H	0.06	0.02	0.04
24C	0.00	0.00	0.00
25H	0.03	0.01	0.02
26H	0.04	0.03	0.03
27H	−0.03	−0.03	−0.03
28C	−0.01	0.85	0.42
29H	0.04	0.02	0.03
30H	0.02	0.01	0.01
31N	−0.02	0.00	−0.01
32C	−0.02	−0.01	−0.01
33H	0.00	0.00	0.00
34C	−0.01	−0.01	−0.01
35C	0.00	0.00	0.00
36C	0.00	0.00	0.00
37C	−0.01	−0.01	−0.01
38H	0.00	0.00	0.00
39C	0.00	0.00	0.00
40C	−0.41	0.42	0.00
41H	−0.01	0.03	0.01
42H	0.09	−0.06	0.01
43Br	0.98	−0.93	0.03
44O	−0.01	−0.01	−0.01
45H	0.01	0.00	0.01

Table 8
Fukui function value of $H2L^2$ molecule.

Atoms	$f+$	f⁻	f
1C	0.02	0.10	0.06
2C	0.01	0.01	0.01
3C	0.01	0.06	0.03
4C	0.02	0.08	0.05
5C	−0.02	−0.12	−0.07
6C	0.02	0.09	0.05
7H	0.04	0.10	0.07
8H	−0.01	0.10	0.05
9H	−0.06	0.09	0.02
10Br	0.10	0.22	0.16
11O	−0.04	0.01	−0.01
12H	0.04	0.03	0.04
13C	−0.11	0.04	−0.03
14H	0.11	0.03	0.07
15N	0.26	−0.03	0.12
16C	−0.26	0.18	−0.04
17H	0.09	0.03	0.06
18H	0.10	0.02	0.06
19C	−0.03	−0.01	−0.02
20C	−0.02	0.00	−0.01
21H	0.04	0.02	0.03
22H	−0.04	−0.03	−0.04
23H	0.06	0.02	0.04
24C	0.00	0.00	0.00
25H	0.03	0.01	0.02
26H	0.04	0.03	0.03
27H	−0.03	−0.03	−0.03
28C	−0.01	0.85	0.42
29H	0.04	0.02	0.03
30N	0.02	0.01	0.01
31N	−0.02	0.00	−0.01
32C	−0.02	−0.01	−0.01
33C	0.00	0.00	0.00
34C	−0.01	−0.01	−0.01
35C	0.00	0.00	0.00
36C	0.00	0.00	0.00
37C	−0.01	−0.01	−0.01
38H	0.00	0.00	0.00
39C	0.00	0.00	0.00
40C	−0.41	0.42	0.00
41H	−0.01	0.03	0.01
42H	0.09	−0.06	0.01
43Br	0.98	−0.93	0.03
44O	−0.01	−0.01	−0.01
45H	0.01	0.00	0.01
46H	0.01	0.00	0.01
47H	0.02	0.01	0.01
48H	0.16	0.00	0.08
49H	0.05	0.07	0.06

$$\text{Temkin}: \theta = \frac{-1}{2a}\ln(K_{ads}) + \frac{-1}{2a}\ln(C_{inh}) \tag{5}$$

$$\text{Freundlich}: \ln\theta = \ln(K_{ads}) + a\ln(C_{inh}) \tag{6}$$

$$\text{Frumkin}: \ln\left(\frac{C_{inh}\theta}{1-\theta}\right) = \ln(K_{ads}) + 2a\theta \tag{7}$$

where θ is the surface coverage of the carbon steel surface measured according to Eq. (3), C_{inh} is the concentration of the $H2L^1$ and $H2L^2$, a is the lateral interaction term and K_{ads} is the adsorption equilibrium constant. Furthermore, K_{ads} has the following relationship with the standard adsorption-free energy (ΔG^0_{ads}).

$$\Delta G^0_{ads} = -RT\ln(55.5K_{ads}) \tag{8}$$

where R and T are the gas constant and temperature in Kelvin. Fig. 10 illustrates the calculated isotherms for $H2L^1$ and $H2L^2$ inhibitors. Also, Table 5 shows the isotherms parameters, ΔG^0_{ads} and the regression coefficient, R^2. The highest values of R^2 with a straight line confirm the best fitting of the isotherm models, which corresponds to Langmuir adsorption isotherm (i.e., 0.9990 for $H2L^1$ and 0.9997 for $H2L^2$). The near-unity slope for carbon steel for $H2L^1$ and $H2L^2$ inhibitors (i.e., slope=1.14 and 1.08, respectively) supports the proposed mechanism in our data.

The K_{ads} calculated for $H2L^1$, and $H2L^2$ inhibitors are 0.23 and 0.42 $(\text{ppm})^{-1}$, respectively. The higher K_{ads} describe the higher fraction coverage of inhibitor molecules. Therefore, inhibitor $H2L^2$ exhibited higher inhibition performance at the exact dosage and condition relative to $H2L^1$. The ΔG^0_{ads}values for $H2L^1$ and $H2L^2$-containing solutions are −11.98 and −13.53 kJ/mol, suggesting that an inhibitor has physically adhered to the metal electrode surface [80].

3.8. Theoretical studies

We can learn more about a variety of properties of molecules via theoretical computations. For this study, a Gauss software package was applied. With the aid of this program, several quantum chemical parameters were derived in the gas and water phases using the B3LYP, HF, and M062X method 6–31++G(d,p) basis sets. We learn about the various chemical characteristics of molecules from each determined quantum chemical parameter (Table 6).

The HOMO and LUMO energy numerical values of the inhibitor compounds are the most crucial and commonly used parameters among

the ones acquired. Because the numerical values represent the compounds' inhibitory actions. The HOMO energy values represent the ability of inhibitor compounds to donate electrons. The LUMO energy value reveals the inhibitor molecules' capacity to receive electrons [51].

Many other characteristics are calculated in addition to these two. The energy difference between the HOMO and LUMO orbitals is expressed, among others, by the gap. This gap is called the ΔE energy gap. Because a low value of this parameter makes it easier for electron transport, the molecule with the lowest numerical value has the most potent inhibitory action [81]. Apart from this parameter, another parameter is the electronegativity of the inhibitor molecules, which is the atoms' power to attract the bonded electrons. When the molecule's electronegativity value increases, the atoms in the molecule will draw the bond electron more strongly, which will cause activity to decrease. Quantum chemical descriptors are compared with each other, and it is found that the anti-corrosive property of $H2L^1$ is better than $H2L^2$ at each calculation level.

Fig. 11 illustrates a mixture of HOMO, LUMO, and ESP (molecular electrostatic potential) inhibitor compounds. The first column displays the optimized structures. The contour plot of HOMO and LUMO are given in the second and third coulomb, respectively. Finally, the ESP diagram is provided in the last coulomb. According to HOMO and LUMO plots, it can be said that π electrons on the benzene ring are active for any interaction.

Furthermore, the volume of the balloons of $H2L^1$ in these plots is more significant than that of $H2L^2$. This situation indicates that $H2L^1$ can easily interact according to $H2L^2$. The final illustration is the ESP diagrams. There are colors on them, and each color has a meaning related to the electron density on the molecular surface. However, electron densities on the molecular surface are similar in studied compounds.

Fukui indices provide information about the tendency of molecules to donate or accept electrons. In addition, it gives important information about which atom in the molecule is suitable for electrophilic or nucleophilic attacks. In the formulas given below, it is possible to define the corresponding condensed or atomic Fukui functions in the atomic domain as follows:

$$\begin{aligned} f_j^+ &= q_j(N+1) - q_j(N) \\ f_j^- &= q_j(N) - q_j(N-1) \\ f_j^0 &= 1/2\left[q_j(N+1) - q_j(N-1)\right] \end{aligned} \tag{9}$$

where for an electrophilic f_j^-(r), nucleophilic or free radical attack f_j^+(r) on the atoms of the reference molecule, respectively. Given in these equations, q_j is the numerical value of the atomic charge in the jth atomic region in neutral (N), anionic $(N+1)$ or cationic (N–1) chemical species (Mulliken population analysis, electrostatic derived charge, etc.). The binary descriptor (Δf(r)), which is defined as the difference between the nucleophilic and electrophilic Fukui function and given by these equations.

If the Δf(r) value is greater than 0, the region is preferred for a nucleophilic attack, while if the Δf(r) value is less than 0, the region is preferred for an electrophilic attack. With respect to the binary identifier, Δf(r) provides a clear distinction between nucleophilic and electrophilic attack at a particular site. as a result, they provide a positive value for atoms prone to nucleophilic attack and a negative value for electrophilic attack. for the molecules studied, the nucleophilic region (Δf(r)>0) is C28 has the highest value with a value of +0.42. and all hydrogen atoms. Similarly, the electrophilic region (Δf(r)<0) is C5 has the lowest value with a value of −0.07 atoms, all calculated values are given in Tables 7 and 8. The behavior of the molecule as electrophilic and nucleophilic attack during the reaction depends on the local behavior of the molecule. The numerical values obtained as a result of the Fukui function analysis were found to be in great agreement with the results of the ESP calculations [82,83].

4. Conclusion

In both static and hydrodynamic settings, the electrochemical behavior of carbon steel in 1.0 M HCl with and without inhibitors was assessed using various approaches. Our investigation's key conclusions are:

1 PDP's data indicates that the solution with 1.0 M HCl (without inhibitors) had the highest i_{corr} value, suggesting the solution with the highest CR compared to solutions containing $H2L^1$ and $H2L^2$.
2 Increasing the concentration of $H2L^1$ from 50 to 250 ppm resulted in a decrease in i_{corr} for carbon steel in solutions containing $H2L^1$ and $H2L^2$. The addition of reduced form $H2L^1$ to the 1.0 M HCl solution produced the best resistance to corrosion compared to solutions without or with $H2L^1$.
3 According to immersion and UV–vis spectroscopy results, 1.0 M HCl solutions with $H2L^1$ and $H2L^2$ inhibitors were added to reduce the carbon steel's corrosion resistance. Among inhibitor-free and inhibitor-containing solutions, the inhibitor $H2L^2$ exhibits the lowest *CR*.
4 The EIS findings show that the $H2L^2$ with a concentration of 250 ppm has an efficiency of over 91.43%.
5 The highest corrosion rate for carbon steel occurred in a hydrodynamic solution without an inhibitor. While adding an inhibitor to the hydrochloric acid solution has significantly reduced the corrosion current, with the lowest value observed in the $H2L^2$ solution.
6 The AFM test results were consistent with both the PDP and EIS tests, indicating that surface roughness was lower under both inhibitors in both static and hydrodynamic conditions.
7 For both $H2L^1$ and $H2L^2$ molecules in the 1.0 M HCl solution, the inhibitor adsorption on the carbon steel surface complies with the Langmuir isotherm.
8 Anti-corrosive properties of studied compounds are investigated in detail computationally. For this aim, different methods were used.

Declaration of Competing Interest

The authors declare that they have no known competing financial interests or personal relationships that could have appeared to influence the work reported in this paper.

References

[1] Alcántara J, de la Fuente D, Chico B, Simancas J, Díaz I, Morcillo M. Marine atmospheric corrosion of carbon steel: a review. Materials 2017;10:406. https://doi.org/10.3390/MA10040406.
[2] Odebiyi OS, Adedayo SM, Tunji LA, Onuorah MO. A review of weldability of carbon steel in arc-based welding processes. Cogent Eng 2019;6. https://doi.org/10.1080/23311916.2019.1609180.
[3] Hegazy MA, El-Etre AY, El-Shafaie M, Berry KM. Novel cationic surfactants for corrosion inhibition of carbon steel pipelines in oil and gas wells applications. J Mol Liq 2016;214:347–56. https://doi.org/10.1016/J.MOLLIQ.2015.11.047.
[4] Naderi J, Sarhan AAD. Measure and evaluate the hardness of the electrodeposited Nickel-Phosphorous (Ni-P) thin film coating on carbon steel alloy for automotive applications. Measurement 2019;139:490–7. https://doi.org/10.1016/J.MEASUREMENT.2019.03.027.
[5] Panossian Z, de Almeida NL, de Sousa RMF, Pimenta G de S, Marques LBS. Corrosion of carbon steel pipes and tanks by concentrated sulfuric acid: a review. Corros Sci 2012;58:1–11. https://doi.org/10.1016/J.CORSCI.2012.01.025.
[6] Naciri M, El Aoufir Y, Lgaz H, Lazrak F, Ghanimi A, Guenbour A, et al. Exploring the potential of a new 1,2,4-triazole derivative for corrosion protection of carbon steel in HCl: a computational and experimental evaluation. Colloids Surf A Physicochem Eng Asp 2020;597:124604. https://doi.org/10.1016/J.COLSURFA.2020.124604.
[7] Dai L, Wang D, Wang T, Feng Q, Yang X. Analysis and comparison of long-distance pipeline failures. J Pet Eng 2017;2017:1–7. https://doi.org/10.1155/2017/3174636.
[8] Zhang S, Hou L, Du H, Wei H, Liu B, Wei Y. A study on the interaction between chloride ions and CO_2 towards carbon steel corrosion. Corros Sci 2020;167:108531. https://doi.org/10.1016/J.CORSCI.2020.108531.
[9] Alrefaee SH, Rhee KY, Verma C, Quraishi MA, Ebenso EE. Challenges and advantages of using plant extract as inhibitors in modern corrosion inhibition

systems: recent advancements. J Mol Liq 2021;321:114666. https://doi.org/10.1016/J.MOLLIQ.2020.114666.
[10] Hajjaji FEL, Salim R, Ech-chihbi E, Titi A, Messali M, Kaya S, et al. New imidazolium ionic liquids as ecofriendly corrosion inhibitors for mild steel in hydrochloric acid (1M): experimental and theoretical approach. J Taiwan Inst Chem Eng 2021;123:346–62. https://doi.org/10.1016/J.JTICE.2021.05.005.
[11] Kadhim A, Al-Amiery AA, Alazawi R, Al-Ghezi MKS, Abass RH. Corrosion inhibitors. A review. Int J Corros Scale Inhib 2021;10:54–67. https://doi.org/10.17675/2305-6894-2021-10-1-3.
[12] Ouass A, Galai M, Ouakki M, Ech-Chihbi E, Kadiri L, Hsissou R, et al. Poly(sodium acrylate) and Poly(acrylic acid sodium) as an eco-friendly corrosion inhibitor of mild steel in normal hydrochloric acid: experimental, spectroscopic and theoretical approach. J Appl Electrochem 2021;51:1009–32. https://doi.org/10.1007/S10800-021-01556-Y/METRICS.
[13] Hsissou R, Benhiba F, Echihi S, Benzidia B, Cherrouf S, Haldhar R, et al. Performance of curing epoxy resin as potential anticorrosive coating for carbon steel in 3.5% NaCl medium: combining experimental and computational approaches. Chem Phys Lett 2021;783:139081. https://doi.org/10.1016/J.CPLETT.2021.139081.
[14] Bedair MA, Soliman SA, Bakr MF, Gad ES, Lgaz H, Chung IM, et al. Benzidine-based Schiff base compounds for employing as corrosion inhibitors for carbon steel in 1.0M HCl aqueous media by chemical, electrochemical and computational methods. J Mol Liq 2020;317:114015. https://doi.org/10.1016/J.MOLLIQ.2020.114015.
[15] Hsissou R, Abbout S, Seghiri R, Rehioui M, Berisha A, Erramli H, et al. Evaluation of corrosion inhibition performance of phosphorus polymer for carbon steel in [1M] HCl: computational studies (DFT, MC and MD simulations). J Mater Res Technol 2020;9:2691–703. https://doi.org/10.1016/J.JMRT.2020.01.002.
[16] Alvarez PE, Fiori-Bimbi MV, Neske A, Brandán SA, Gervasi CA. Rollinia occidentalis extract as green corrosion inhibitor for carbon steel in HCl solution. J Ind Eng Chem 2018;58:92–9. https://doi.org/10.1016/J.JIEC.2017.09.012.
[17] Wang Q, Tan B, Bao H, Xie Y, Mou Y, Li P, et al. Evaluation of Ficus tikoua leaves extract as an eco-friendly corrosion inhibitor for carbon steel in HCl media. Bioelectrochemistry 2019;128:49–55. https://doi.org/10.1016/J.BIOELECHEM.2019.03.001.
[18] Jokar M, Farahani TS, Ramezanzadeh B. Electrochemical and surface characterizations of morus alba pendula leaves extract (MAPLE) as a green corrosion inhibitor for steel in 1M HCl. J Taiwan Inst Chem Eng 2016;63:436–52. https://doi.org/10.1016/J.JTICE.2016.02.027.
[19] Ji G, Anjum S, Sundaram S, Prakash R. Musa paradisica peel extract as green corrosion inhibitor for mild steel in HCl solution. Corros Sci 2015;90:107–17. https://doi.org/10.1016/J.CORSCI.2014.10.002.
[20] Swaroop BS, Victoria SN, Manivannan R. Azadirachta indica leaves extract as inhibitor for microbial corrosion of copper by Arthrobacter sulfureus in neutral pH conditions—A remedy to blue green water problem. J Taiwan Inst Chem Eng 2016;64:269–78. https://doi.org/10.1016/J.JTICE.2016.04.007.
[21] Sedik A, Lerari D, Salci A, Athmani S, Bachari K, Gecibesler H, et al. Dardagan Fruit extract as eco-friendly corrosion inhibitor for mild steel in 1M HCl: electrochemical and surface morphological studies. J Taiwan Inst Chem Eng 2020;107:189–200. https://doi.org/10.1016/J.JTICE.2019.12.006.
[22] El Faydy M, Galai M, El Assyry A, Tazouti A, Touir R, Lakhrissi B, et al. Experimental investigation on the corrosion inhibition of carbon steel by 5-(chloromethyl)-8-quinolinol hydrochloride in hydrochloric acid solution. J Mol Liq 2016;219:396–404. https://doi.org/10.1016/J.MOLLIQ.2016.03.056.
[23] Zarrouk A, Hammouti B, Lakhlifi T, Traisnel M, Vezin H, Bentiss F. New 1H-pyrrole-2,5-dione derivatives as efficient organic inhibitors of carbon steel corrosion in hydrochloric acid medium: electrochemical, XPS and DFT studies. Corros Sci 2015;90:572–84. https://doi.org/10.1016/J.CORSCI.2014.10.052.
[24] Ouakki M, Galai M, Benzekri Z, Aribou Z, Ech-chihbi E, Guo L, et al. A detailed investigation on the corrosion inhibition effect of by newly synthesized pyran derivative on mild steel in 1.0M HCl: experimental, surface morphological (SEM-EDS, DRX& AFM) and computational analysis (DFT & MD simulation). J Mol Liq 2021;344:117777. https://doi.org/10.1016/J.MOLLIQ.2021.117777.
[25] Ouakki M, Galai M, Aribou Z, Benzekri Z, El Assiri EH, Dahmani K, et al. Detailed experimental and computational explorations of pyran derivatives as corrosion inhibitors for mild steel in 1.0M HCl: electrochemical/surface studies, DFT modeling, and MC simulation. J Mol Struct 2022;1261:132784. https://doi.org/10.1016/J.MOLSTRUC.2022.132784.
[26] Galai M, Rbaa M, Ouakki M, Dahmani K, Kaya S, Arrousse N, et al. Functionalization effect on the corrosion inhibition of novel eco-friendly compounds based on 8-hydroxyquinoline derivatives: experimental, theoretical and surface treatment. Chem Phys Lett 2021;776:138700. https://doi.org/10.1016/J.CPLETT.2021.138700.
[27] Galai M, Rbaa M, Ouakki M, Guo L, Dahmani K, Nouneh K, et al. Effect of alkyl group position on adsorption behavior and corrosion inhibition of new naphthol based on 8-hydroxyquinoline: electrochemical, surface, quantum calculations and dynamic simulations. J Mol Liq 2021;335:116552. https://doi.org/10.1016/J.MOLLIQ.2021.116552.
[28] Fouda AS, El-Ewady G, Ali AH. Modazar as promising corrosion inhibitor of carbon steel in hydrochloric acid solution. Green Chem Lett Rev 2017;10:88–100. https://doi.org/10.1080/17518253.2017.1299228.
[29] Chauhan DS, Quraishi MA, Sorour AA, Saha SK, Banerjee P. Triazole-modified chitosan: a biomacromolecule as a new environmentally benign corrosion inhibitor for carbon steel in a hydrochloric acid solution. RSC Adv 2019;9:14990–5003. https://doi.org/10.1039/C9RA00986H.
[30] Dewangan AK, Dewangan Y, Verma DK, Verma C. Synthetic environment-friendly corrosion inhibitors. Environ Sustain Corros Inhib 2022:71–95. https://doi.org/10.1016/B978-0-323-85405-4.00020-3.
[31] Hegazy MA, Hasan AM, Emara MM, Bakr MF, Youssef AH. Evaluating four synthesized Schiff bases as corrosion inhibitors on the carbon steel in 1M hydrochloric acid. Corros Sci 2012;65:67–76. https://doi.org/10.1016/J.CORSCI.2012.08.005.
[32] Rezaeivala M, Keypour H, Salehzadeh S, Latifi R, Chalabian F, Katouzian F. Synthesis, characterization and crystal structure of some new Mn(II) and Zn(II) macroacyclic Schiff base complexes derived from two new asymmetrical (N5) branched amines and pyridine-2-carbaldehyde or O-vaniline and their antibacterial properties. J Iran Chem Soc 2014;11:431–40. https://doi.org/10.1007/S13738-013-0315-4.
[33] Keypour H, Shayesteh M, Rezaeivala M, Dhers S, Küp FÖ, Güllü M, et al. Mononuclear Ni(II) complexes of Schiff base ligands formed from unsymmetrical tripodal amines of differing arm lengths: spectral, X-ray crystal structural, antimicrobial and DNA cleavage activity. J Mol Struct 2017;1148:568–76. https://doi.org/10.1016/J.MOLSTRUC.2017.07.058.
[34] Rezaeivala M, Golbedaghi R, Khalili M, Ahmad M, Sayin K, Chalabian F. The different effects of metal ions on the synthesis of macroacyclic compounds: x-ray crystal structure, theoretical studies, antibacterial and antifungal activities. Russ J Coord Chem Koordinatsionnaya Khimiya 2019;45:142–53. https://doi.org/10.1134/S1070328419020064.
[35] Rezaeivala M, Ahmadi M, Captain B, Şahin-Bölükbaşı S, Dehghani-Firouzabadi AA, William Gable R. Synthesis, characterization, and cytotoxic activity studies of new N4O complexes derived from 2-({3-[2-*morpholinoethylamino*]-N3-([*pyridine*-2-*yl*]methyl) propylimino} methyl)phenol. Appl Organomet Chem 2020;34:e5325. https://doi.org/10.1002/AOC.5325.
[36] Rezaeivala M, Ahmadi M, Captain B, Bayat M, Saeidirad M, Şahin-Bölükbaşı S, et al. Some new morpholine-based Schiff-base complexes; Synthesis, characterization, anticancer activities and theoretical studies. Inorg Chim Acta 2020;513:119935. https://doi.org/10.1016/J.ICA.2020.119935.
[37] Afkhami A, Soltani-Felehgari F, Madrakian T, Ghaedi H, Rezaeivala M. Fabrication and application of a new modified electrochemical sensor using nano-silica and a newly synthesized Schiff base for simultaneous determination of Cd^{2+}, Cu^{2+} and Hg^{2+} ions in water and some foodstuff samples. Anal Chim Acta 2013;771:21–30. https://doi.org/10.1016/J.ACA.2013.02.031.
[38] Jafari H, Rezaeivala M, Mokhtarian N, Berisha A, Ameri E. Corrosion Inhibition of Carbon Steel in 0.5M H_2SO_4 by new reduced Schiff base ligand. J Bio Tribocorros 2022;8:1–13. https://doi.org/10.1007/S40735-022-00679-9/METRICS.
[39] Jafari H, Ameri E, Rezaeivala M, Berisha A. Experimental and theoretical studies on protecting steel against 0.5M H_2SO_4 corrosion by new schiff base. J Indian Chem Soc 2022;99:100665. https://doi.org/10.1016/J.JICS.2022.100665.
[40] Jafari H, Ameri E, Rezaeivala M, Berisha A. 4,4'-(((2,2-Dimethylpropane-1,3-Diyl) Bis(Azanediyl)Bis(Methylene) Bis(2-Methoxyphenol) as new reduced form of schiff base for protecting API 5L Grade B in 1M HCl. Arab J Sci Eng 2022:1–14. https://doi.org/10.1007/S13369-022-07281-8/METRICS.
[41] Jafari H, Ameri E, Rezaeivala M, Berisha A, Vakili MH. Comparison the anticorrosion behavior of three symmetrical Schiff-base ligands: experimental and theoretical studies. J Appl Electrochem 2022;52:1803–18. https://doi.org/10.1007/S10800-022-01748-0/METRICS.
[42] Shetty P. Schiff bases: an overview of their corrosion inhibition activity in acid media against mild steel. Chem Eng Commun 2019;207:985–1029. https://doi.org/10.1080/00986445.2019.1630387.
[43] Verma C, Quraishi MA. Recent progresses in Schiff bases as aqueous phase corrosion inhibitors: design and applications. Coord Chem Rev 2021;446:214105. https://doi.org/10.1016/J.CCR.2021.214105.
[44] El Basiony NM, Elgendy A, Nady H, Migahed MA, Zaki EG. Adsorption characteristics and inhibition effect of two Schiff base compounds on corrosion of mild steel in 0.5M HCl solution: experimental, DFT studies, and Monte Carlo simulation. RSC Adv 2019;9:10473–85. https://doi.org/10.1039/C9RA00397E.
[45] Jamil DM, Al-Okbi AK, SB Al-B, Al-Amiery AA, Kadhim A, Gaaz TS, et al. Experimental and theoretical studies of Schiff bases as corrosion inhibitors. Chem Cent J 2018;12:1–9. https://doi.org/10.1186/S13065-018-0376-7/TABLES/4.
[46] Soltani N, Salavati H, Rasouli N, Paziresh M, Moghadasi A. Adsorption and corrosion inhibition effect of schiff base ligands on low carbon steel corrosion in hydrochloric acid solution. Chem Eng Commun 2016;203:840–54. https://doi.org/10.1080/00986445.2015.1076801.
[47] Verma C, Olasunkanmi LO, Ebenso EE, Quraishi MA. Substituents effect on corrosion inhibition performance of organic compounds in aggressive ionic solutions: a review. J Mol Liq 2018;251:100–18. https://doi.org/10.1016/J.MOLLIQ.2017.12.055.
[48] Chen S, Pudukudy M, Yue Z, Zhang H, Zhi Y, Ni Y, et al. Nonmetal Schiff-base complex-anchored cellulose as a novel and reusable catalyst for the solvent-free ring-opening addition of CO_2 with epoxides. Ind Eng Chem Res 2019;58:17255–65. https://doi.org/10.1021/ACS.IECR.9B03331/SUPPL_FILE/IE9B03331_SI_001.PDF.
[49] Şafak S, Duran B, Yurt A, Türkoğlu G. Schiff bases as corrosion inhibitor for aluminium in HCl solution. Corros Sci 2012;54:251–9. https://doi.org/10.1016/J.CORSCI.2011.09.026.
[50] Umoren SA, Solomon MM. Effect of halide ions on the corrosion inhibition efficiency of different organic species – a review. J Ind Eng Chem 2015;21:81–100. https://doi.org/10.1016/J.JIEC.2014.09.033.
[51] Kafa AHT, Tüzün G, Güney E, Aslan R, Sayın K, Tüzün B, et al. Synthesis, computational analyses, antibacterial and antibiofilm properties of nicotinamide

derivatives. Struct Chem 2022;33:1189–97. https://doi.org/10.1007/S11224-022-01927-X/METRICS.
[52] Rezaeivala M, Karimi S, Sayin K, Tüzün B. Experimental and theoretical investigation of corrosion inhibition effect of two piperazine-based ligands on carbon steel in acidic media. Colloids Surf A Physicochem Eng Asp 2022;641:128538. https://doi.org/10.1016/J.COLSURFA.2022.128538.
[53] Dennington R, Keith T, Millam J. Gauss view, version 5. Shawnee Mission: Semichem Inc.; 2009. - References - Scientific Research Publishing n.d. https://www.scirp.org/(S(vtj3fa45qm1ean45vvffcz55))/reference/ReferencesPapers.aspx?ReferenceID=1958990. accessed February 11, 2023
[54] LastNameFrisch M.J.T, et al., (2009) Gaussian 09. revision D01 Gaussian Inc, Wallingford CT n.d.
[55] Becke AD. Density-functional thermochemistry. I. The effect of the exchange-only gradient correction. J Chem Phys 1998;96:2155. https://doi.org/10.1063/1.462066.
[56] Vautherin D, Brink DM. Hartree-Fock Calculations with Skyrme's Interaction. I. Spherical Nuclei. Phys Rev C 1972;5:626. https://doi.org/10.1103/PhysRevC.5.626.
[57] Hohenstein EG, Chill ST, Sherrill CD. Assessment of the performance of the M05#2X and M06#2X exchange correlation functionals for noncovalent interactions in biomolecules. J Chem Theory Comput 2008;4:1996–2000. https://doi.org/10.1021/CT800308K/SUPPL_FILE/CT800308K_SI_001.PDF.
[58] Karimi S, Rezaeivala M, Sayin K, Tuzun B. Experimental and computational investigation of 3,5-di-tert-butyl-2-(((3-((2-morpholinoethyl)(pyridin-2-ylmethyl)amino)propyl)imino) methyl)phenol and related reduced form as an inhibitor for C-steel. Mater Chem Phys 2022;287:126152. https://doi.org/10.1016/J.MATCHEMPHYS.2022.126152.
[59] Kalkhambkar AG, Rajappa SK. Effect of Schiff's bases on corrosion protection of mild steel in hydrochloric acid medium: electrochemical, quantum chemical and surface characterization studies. Chem Eng J Adv 2022;12:100407. https://doi.org/10.1016/J.CEJA.2022.100407.
[60] Li E, Li Y, Liu S, Yao P. Choline amino acid ionic liquids as green corrosion inhibitors of mild steel in acidic medium. Colloids Surf A Physicochem Eng Asp 2023;657:130541. https://doi.org/10.1016/J.COLSURFA.2022.130541.
[61] Han T, Guo J, Zhao Q, Wu Y, Zhang Y. Enhanced corrosion inhibition of carbon steel by pyridyl gemini surfactants with different alkyl chains. Mater Chem Phys 2020;240:122156. https://doi.org/10.1016/J.MATCHEMPHYS.2019.122156.
[62] Rbaa M, Benhiba F, Abousalem AS, Galai M, Rouifi Z, Oudda H, et al. Sample synthesis, characterization, experimental and theoretical study of the inhibitory power of new 8-hydroxyquinoline derivatives for mild steel in 1.0M HCl. J Mol Struct 2020;1213:128155. https://doi.org/10.1016/J.MOLSTRUC.2020.128155.
[63] Rbaa M, Dohare P, Berisha A, Dagdag O, Lakhrissi L, Galai M, et al. New Epoxy sugar based glucose derivatives as eco friendly corrosion inhibitors for the carbon steel in 1.0M HCl: experimental and theoretical investigations. J Alloys Compd 2020;833:154949. https://doi.org/10.1016/J.JALLCOM.2020.154949.
[64] Emregül KC, Atakol O. Corrosion inhibition of iron in 1M HCl solution with Schiff base compounds and derivatives. Mater Chem Phys 2004;83:373–9. https://doi.org/10.1016/J.MATCHEMPHYS.2003.11.008.
[65] da Silva AB, D'Elia E, da Cunha Ponciano Gomes JA. Carbon steel corrosion inhibition in hydrochloric acid solution using a reduced Schiff base of ethylenediamine. Corros Sci 2010;52:788–93.
[66] Rihan R, Shawabkeh R, Al-Bakr N. The effect of two amine-based corrosion inhibitors in improving the corrosion resistance of carbon steel in sea water. J Mater Eng Perform 2014;23:693–9. https://doi.org/10.1007/s11665-013-0790-x.
[67] El-Azabawy OE, Higazy SA, Al-Sabagh AM, Abdel-Rahman AAH, Nasser NM, Khamis EA. Studying the temperature influence on carbon steel in sour petroleum media using facilely-designed Schiff base polymers as corrosion inhibitors. J Mol Struct 2023;1275:134518. https://doi.org/10.1016/J.MOLSTRUC.2022.134518.
[68] Chen W, Nie B, Liu M, Li HJ, Wang DY, Zhang W, et al. Mitigation effect of quinazolin-4(3H)-one derivatives on the corrosion behaviour of mild steel in HCl. Colloids Surf A Physicochem Eng Asp 2021;627:127188. https://doi.org/10.1016/j.colsurfa.2021.127188.
[69] Long WJ, Li XQ, Xu P, Feng GL, He C. Facile and scalable preparation of carbon dots with Schiff base structures toward an efficient corrosion inhibitor. Diam Relat Mater 2022;130:109401. https://doi.org/10.1016/J.DIAMOND.2022.109401.
[70] Li XL, Xie B, Feng JS, Lai C, Bai XX, Li T, et al. 2-Pyridinecarboxaldehyde-based Schiff base as an effective corrosion inhibitor for mild steel in HCl medium: experimental and computational studies. J Mol Liq 2022;345:117032. https://doi.org/10.1016/J.MOLLIQ.2021.117032.
[71] Rbaa M, Benhiba F, Dohare P, Lakhrissi L, Touir R, Lakhrissi B, et al. Synthesis of new epoxy glucose derivatives as a non-toxic corrosion inhibitors for carbon steel in molar HCl: experimental, DFT and MD simulation. Chem Data Collect 2020;27:100394. https://doi.org/10.1016/J.CDC.2020.100394.
[72] Ashassi-Sorkhabi H, Ghasemi Z, Seifzadeh D. The inhibition effect of some amino acids towards the corrosion of aluminum in 1M HCl + 1M H_2SO_4 solution. Appl Surf Sci 2005;249:408–18. https://doi.org/10.1016/j.apsusc.2004.12.016.
[73] Askari M, Aliofkhazraei M, Ghaffari S, Hajizadeh A. Film former corrosion inhibitors for oil and gas pipelines - a technical review. J Nat Gas Sci Eng 2018;58:92–114. https://doi.org/10.1016/J.JNGSE.2018.07.025.
[74] Onyeachu IB, Obot IB, Alamri AH, Eziukwu CA. Effective acid corrosion inhibitors for X60 steel under turbulent flow condition based on benzimidazoles: electrochemical, theoretical, SEM, ATR-IR and XPS investigations. Eur Phys J Plus 2020;135:129. https://doi.org/10.1140/EPJP/S13360-020-00167-4.
[75] Obot IB, Onyeachu IB, Umoren SA. Alternative corrosion inhibitor formulation for carbon steel in CO_2-saturated brine solution under high turbulent flow condition for use in oil and gas transportation pipelines. Corros Sci 2019;159:108140. https://doi.org/10.1016/J.CORSCI.2019.108140.
[76] Barmatov E, Hughes TL. Effect of corrosion products and turbulent flow on inhibition efficiency of propargyl alcohol on AISI 1018 mild carbon steel in 4M hydrochloric acid. Corros Sci 2017;123:170–81. https://doi.org/10.1016/J.CORSCI.2017.04.020.
[77] Abderrazak H, Dachraoui M, Lendl B. A novel flow injection procedure for determination of phosphate in industrial raw phosphoric acid. Analyst 2000;125:1211–3. https://doi.org/10.1039/B001208O.
[78] Hsissou R, Benhiba F, El Aboubi M, Abbout S, Benzekri Z, Safi Z, et al. Synthesis and performance of two ecofriendly epoxy resins as a highly efficient corrosion inhibition for carbon steel in 1M HCl solution: DFT, RDF, FFV and MD approaches. Chem Phys Lett 2022;806:139995. https://doi.org/10.1016/J.CPLETT.2022.139995.
[79] Benhiba F, Hsissou R, Benzikri Z, Echihi S, El-Blilak J, Boukhris S, et al. DFT/electronic scale, MD simulation and evaluation of 6-methyl-2-(p-tolyl)-1,4-dihydroquinoxaline as a potential corrosion inhibition. J Mol Liq 2021;335:116539. https://doi.org/10.1016/J.MOLLIQ.2021.116539.
[80] Kumar H, Yadav V, Anu Kr, Saha S, Kang N. Adsorption and inhibition mechanism of efficient and environment friendly corrosion inhibitor for mild steel: experimental and theoretical study. J Mol Liq 2021;338:116634. https://doi.org/10.1016/J.MOLLIQ.2021.116634.
[81] Rezaeivala M, Karimi S, Tuzun B, Sayin K. Anti-corrosion behavior of 2-((3-(2-morpholino ethylamino) -N3-((pyridine-2-yl)methyl)propylimino)methyl)pyridine and its reduced form on Carbon Steel in Hydrochloric Acid solution: experimental and theoretical studies. Thin Solid Films 2022;741:139036. https://doi.org/10.1016/J.TSF.2021.139036.
[82] Saravanan S, Balachandran V. Conformational stability, spectroscopic (FT-IR, FT-Raman and UV–Vis) analysis, NLO, NBO, FMO and Fukui function analysis of 4-hexylacetophenone by density functional theory. Spectrochim Acta A Mol Biomol Spectrosc 2015;138:406–23. https://doi.org/10.1016/j.saa.2014.11.091.
[83] Demircioğlu Z, Kaştaş ÇA, Büyükgüngör O. X-ray structural, spectroscopic and computational approach (NBO, MEP, NLO, NPA, fukui function analyses) of (E)-2-((4-bromophenylimino)methyl)-3-methoxyphenol. Mol Cryst Liq Cryst 2017;656:169–84. https://doi.org/10.1080/15421406.2017.1405660.